

<https://doi.org/10.1038/s42005-024-01543-7>

Strain engineering of nonlinear nanoresonators from hardening to softening

Check for updates

Zichao Li¹ , Minxing Xu^{1,2}, Richard A. Norte^{1,2}, Alejandro M. Aragón¹, Peter G. Steeneken^{1,2} & Farbod Alijani¹

Although strain engineering and soft-clamping techniques for attaining high Q -factors in nanoresonators have received much attention, their impact on nonlinear dynamics is not fully understood. In this study, we show that nonlinearity of high- Q Si_3N_4 nanomechanical string resonators can be substantially tuned by support design. Through careful engineering of support geometries, we control both stress and mechanical nonlinearities, effectively tuning nonlinear stiffness of two orders of magnitude. Our approach also allows control over the sign of the Duffing constant resulting in nonlinear softening of the mechanical mode that conventionally exhibits hardening behavior. We elucidate the influence of support design on the magnitude and trend of the nonlinearity using both analytical and finite element-based reduced-order models that validate our experimental findings. Our work provides evidence of the role of soft-clamping on the nonlinear dynamic response of nanoresonators, offering an alternative pathway for nullifying or enhancing nonlinearity in a reproducible and passive manner.

High- Q nanomechanical resonators play a central role in sensing and enable ultrasmall mass, acceleration, and force detection. Nonetheless, due to their nanoscale size and exceptional isolation from the surrounding environment, even minute forces, as small as a few piconewtons, can induce large-amplitude oscillations in them and result in a plethora of nonlinear phenomena that include bi-stability^{1–4}, parametric resonance^{5–7}, self-oscillations^{8–10}, and mode-coupling^{11–14}. Many of these nonlinear phenomena can provide new information that is absent in the linear regime of operation. For instance, nonlinear resonances can be used to characterize nanomaterial properties^{15,16}, enhance frequency stability^{12,17}, or generate mechanical frequency combs^{18,19}. Some of these nonlinear phenomena have been engineered by leveraging the interplay between geometric and electrostatic nonlinearities^{6,20}. However, the introduction of external competing nonlinear forces may give rise to a series of unwanted side-effects, including noise^{21,22} or back-action effects²³ that can further complicate the nonlinear dynamic behavior, device fabrication, and operation. Therefore, methodologies that can tailor the dynamic characteristics of nanomechanical devices solely through geometric design in the fabrication stage are highly desirable.

Although numerous studies have already demonstrated the design optimization of resonance frequencies and Q -factor of nanomechanical

resonators^{24–29}, the influence of geometric design on nonlinear dynamics has rarely been investigated^{11,30,31}. Here, we show that soft-clamping techniques that are utilized to realize high- Q nanomechanical resonators can also be engineered to tune nonlinear dynamics. By manipulating the support boundary in high-stress Si_3N_4 string resonators, we can tune the stress field and induce strong in-plane to out-of-plane coupling to simultaneously increase the Q -factor and the onset of nonlinearity over three times that of a doubly clamped string. Furthermore, by changing the support angle, we show that it is possible to engineer compressive forces in the soft-clamped resonators and achieve buckled configurations in a controllable manner. These buckled states allow us to maximize geometric nonlinearity and change the response from hardening to softening. To understand the conditions required for strain engineering and buckling, we develop reduced-order models from finite element (FE) simulations, which highlight the role of the support angle in tuning the nonlinear dynamic response. Our results thus provide experimental evidence of controllable nonlinear dynamic engineering of nanomechanical resonators solely by geometric design and pave the way for integrating arrays of highly tunable nonlinear nanodevices on a single chip^{32–36}.

¹Department of Precision and Microsystems Engineering, Delft University of Technology, Mekelweg 2, 2628 CD Delft, The Netherlands. ²Kavli Institute of Nanoscience, Delft University of Technology, Lorentzweg 1, 2628 CJ Delft, The Netherlands. e-mail: z.li-16@tudelft.nl; f.alijani@tudelft.nl

Results

Nonlinear dynamic characterization

Figure 1a shows a scanning electron microscope (SEM) image of a nanomechanical resonator we fabricated with high-stress Si₃N₄ (see “Methods” for more details). The central string resonator of all studied devices had the same length ($L = 200 \mu\text{m}$) and width ($w = 2 \mu\text{m}$). However, the geometric parameters of the support beams, namely the support length L_s , the width w_s , and the angle θ (see Fig. 1b), are varied to investigate their effect on the nonlinear response. To characterize the nonlinear dynamics of the string resonators, we fix a chip with nanodevices to a piezo actuator that provides harmonic drive in the out-of-plane direction. We use a Zurich Instruments HF2LI lock-in amplifier connected to an MSA400 Polytec Laser Doppler Vibrometer that is focused at the center of the string resonator to carry out frequency sweeps (see Fig. 1c). We perform all the measurements at room temperature and in vacuum chamber with pressure below 2×10^{-6} mbar to improve the signal-to-noise ratio and minimize air damping.

To probe the geometric nonlinearity of our devices, we conduct frequency sweeps at different drive levels and measure the vibrations of the central string. Fig. 1d shows the frequency response at various drive levels for a device with $\theta = 0$. We note the presence of a hardening-type nonlinearity at large amplitudes that arises from the elongation of the string during vibrations. To quantify the observed nonlinearity, we use the Duffing equation:

$$\ddot{q} + \mu\dot{q} + \alpha q + \beta q^3 = F_{\text{exc}} \sin(2\pi ft). \quad (1)$$

where q is the displacement of the center of the string, $F_{\text{exc}} \sin(2\pi ft)$ is the mass normalized harmonic drive force, $\alpha = (2\pi f_0)^2$, $\mu = 2\pi f_0/Q$ are the mass-normalized linear stiffness damping coefficient, respectively. Furthermore, β is the Duffing constant that we extract by fitting the backbone of the experimental frequency response curves using the expression: $f_{\text{max}}^2 = f_0^2 + \frac{3}{16\pi^2} \beta A_{\text{max}}^2$, where f_{max} is the drive frequency corresponding to the maximum amplitude A_{max} ^{37,38} (see Supplementary Note 1). In Fig. 1e, we quantify the change in the Duffing constant β when varying the support length L_s with $\theta = 0$. We observe a factor 13 reduction in the extracted β

when increasing the support length L_s from $30 \mu\text{m}$ to $150 \mu\text{m}$. This is because long supports offer less rigidity to the in-plane motion, thus allowing the central string to relax when vibrating at large amplitudes and consequently reducing the overall geometric nonlinearity.

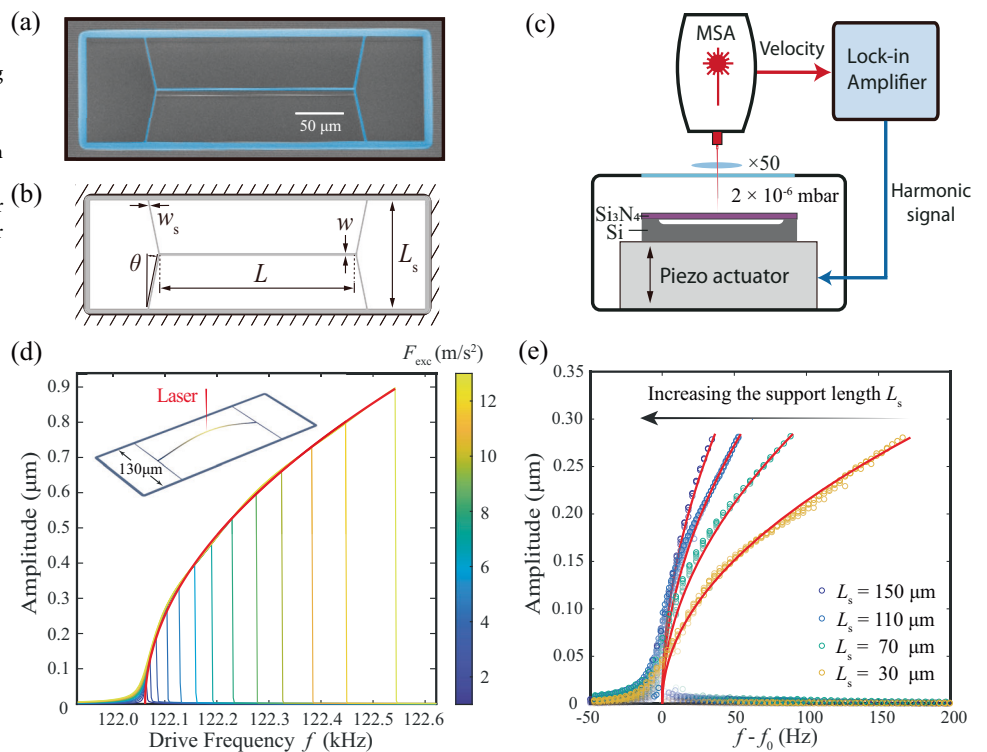
Theoretical model showing the influence of soft-clamping

The reduction in the Duffing constant observed in Fig. 1e highlights the role of the in-plane stiffness on the geometric nonlinearity. Hence, to better understand the influence of support stiffness, we perform additional experiments on a large number of string resonators with different support length L_s and width w_s and extract their Duffing constant β . Moreover, we develop a simplified model consisting of a string connected to in-plane springs at both ends, denoted as k_{in} (see Fig. 2a), to quantitatively capture the influence of L_s and w_s on k_{in} and thus on β when $\theta = 0$. We particularly model the boundary springs as doubly clamped beams with pre-tension $\sigma_0 = 1.06 \text{ GPa}$ and use their central deflection to analytically estimate k_{in} as follows²⁹:

$$k_{\text{in}} = (k_{\text{Ei}}^{-1} + k_{\text{si}}^{-1})^{-1} + k_{\text{oi}} = \left[\left(\frac{16Ehw_s^3}{L_s^3} \right)^{-1} + \left(\frac{2Ehw_s}{(1+\nu)\eta L_s} \right)^{-1} \right]^{-1} + \frac{4\sigma_0 h w_s}{L_s}, \quad (2)$$

where k_{Ei} is the bending stiffness, k_{si} is the shear stiffness, k_{oi} is the additional contribution from the pre-tension. Moreover, η is a geometric factor that, for a rectangular cross-section, is $\eta = 1.2$ ³⁹. In contrast to the central part, which is assumed to be a vibrating string, the support beam is modeled as a moderately thick beam ($w_s/h \geq 2.94$), for estimating k_{in} . To validate our analytical estimation of the in-plane stiffness k_{in} , we also obtained it numerically using FE simulations. The analytical (lines) and the FE (circles) results in Fig. 2b closely match one another and confirm our earlier prediction that wider and shorter support beams offer more rigidity against the deflection, particularly in the in-plane direction. Next, to capture the effect of in-plane springs on the in-plane to out-of-plane coupling and thus nonlinear dynamics, we obtain the Lagrangian $\mathcal{L} = T - U_s - U_k$, where T is the kinetic energy of the string, U_s and U_k are the potential energy of the

Fig. 1 | Nonlinear dynamic characterization of string nanoresonators. **a** Scanning electron microscope (SEM) image, colored in blue, of a string resonator with $L_s = 110 \mu\text{m}$, $\theta = 0.2$ rad. **b** Illustration of design parameters. **c** Schematic of the measurement set-up comprising a Micro System Analyzer (MSA) Laser Doppler Vibrometer (LDV) for reading out the motion and a piezo-actuator for generating the excitation force. **d** Duffing nonlinear response of the string resonator with $w_s = 1 \mu\text{m}$, $L_s = 130 \mu\text{m}$, and $\theta = 0$ as a function of the drive level. **e** Sensitivity of the Duffing response to the support length L_s for string resonators with $w_s = 1 \mu\text{m}$ and $\theta = 0$. The measurements are conducted on four string resonators with different L_s marked with different colors. The fitted backbone curves are shown in red, and the fitted β values for $L_s = (30, 70, 110, 150) \mu\text{m}$ are $\beta = (8.28, 2.12, 0.96, 0.62) \times 10^{22} \text{ m}^{-2} \text{ s}^{-2}$, respectively. The mass normalized excitation levels F_{exc} in (c) and (d) are indicated by the color scale.



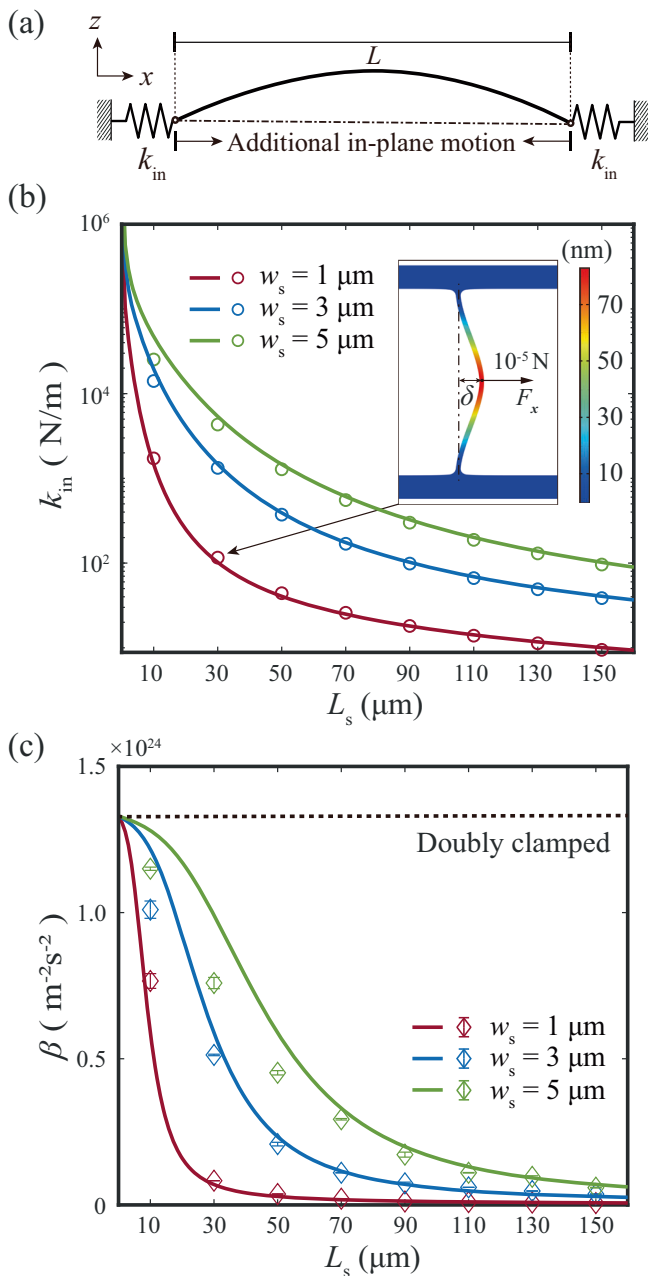


Fig. 2 | Influence of in-plane stiffness on the geometric nonlinearity of string resonators. **a** Simplified model of a string vibrating in the out-of-plane direction, denoted as z , with finite in-plane stiffness k_{in} . **b** Analytical (solid lines) and finite element (FE) based (circles and inset) results of the in-plane stiffness k_{in} for a support beam with varying L_s and w_s . **c** Analytical (solid lines) and measured (diamonds) β of a string resonator with varying L_s and w_s corresponding to (b). The dashed line shows the analytical estimation of β for a doubly clamped string resonator.

string and the two springs k_{in} , respectively, and use Lagrange equations to obtain the updated α and β as follows (see Supplementary Note 2 for details):

$$\alpha = \frac{k_1}{m_{eff}} = \frac{\pi^2(1-\nu)\sigma_0}{\rho L^2} \left(1 + \frac{2EA}{k_{in}L}\right)^{-1}, \quad (3)$$

$$\beta = \frac{k_3}{m_{eff}} = \frac{\pi^4 E}{4\rho L^4} \left(1 + \frac{2EA}{k_{in}L}\right)^{-1}, \quad (4)$$

where k_1 and k_3 are the linear stiffness and the Duffing constant before mass normalization, respectively, $m_{eff} = \rho AL/2$ is the effective mass, and $A = hw$ is the area of the string's cross-section. It is worth noting that $(1 + 2EA/k_{in}L)^{-1}$ serves as a tuning factor introduced by the finite in-plane stiffness k_{in} , which changes both α and β of a doubly clamped string with stress at the same rate. The effect of k_{in} on the nonlinear stiffness can intuitively be understood by realizing that the geometric nonlinear stiffness of a string resonator is due to the increase of average string length and the resulting tension proportional to q^2 . If the clamping at the ends of the string is weakened by reducing the value of springs k_{in} , then the tension increase for the same length increase will be less, such that the nonlinear stiffness β will reduce, as shown by Eq. (4).

In Fig. 2c, we show the extracted Duffing constant β from experiments via fitting the backbone curves of the frequency responses and compare them to the analytical model predictions from Eq. (4). From Fig. 2b and Fig. 2c, it is apparent that the variation in β matches the model quite well. We shall note that for the tested device with the slenderest support ($L_s = 150 \mu\text{m}$, $w_s = 1 \mu\text{m}$) and the central string stress of 5.08 MPa, the analytically derived $f_0 = 94 \text{ kHz}$ and $\beta = 7.21 \times 10^{21} \text{ m}^{-2} \text{ s}^{-2}$ compare well with the measured counterparts $f_0 = 103 \text{ kHz}$ and $\beta = 6.20 \times 10^{21} \text{ m}^{-2} \text{ s}^{-2}$. Therefore, the assumptions of having high-stress strings with sinusoidal eigenmode are valid for obtaining the analytical expressions in the case of $\theta = 0$. By comparing the dashed line to the experimental values in Fig. 2c, it can be seen that the geometric nonlinearity β can be reduced by up to two orders of magnitude using the presented support design. This substantial reduction in geometric nonlinearity highlights the role of support design in tailoring nonlinear dynamic behaviors in nanomechanical resonators with soft-clamping. It is also noteworthy that the β calculated by using the simplified model converges to the value of a doubly clamped string ($1.33 \times 10^{24} \text{ m}^{-2} \text{ s}^{-2}$) when the support length L_s tends to zero (k_{in} approaches infinity in Eq. (4)), thus further confirming our model. However, in the case of wider and shorter supports, we notice that the simplified model deviates from the measurements. We attribute this to the fact that the dimensions of the supports become comparable to the underetch distance of the Si_3N_4 ($\sim 5 \mu\text{m}$) such that the assumptions used for the derivation of Eq. (2) might not be valid anymore.

Engineering the nonlinearity from hardening to buckling-induced softening

To gain a deeper understanding of the full potential of support design on nonlinear dynamics, we also look into the influence of the support angle θ on the nonlinear frequency response curves. By changing θ from positive to negative, we are able to tune the tilting direction of the backbone curves around the resonance, from the common hardening nonlinearity to softening (see Fig. 3a). To understand the physical mechanism behind this observation; we use Keyence Digital Microscope VHX-6000 to focus at the middle of central string and the unreleased Si_3N_4 layer to measure the difference H of their focal heights, as shown in Fig. 3b. We note a maximum deviation of $H = 22.17 \mu\text{m}$ for the device with $L_s = 150 \mu\text{m}$ and $\theta = -0.1 \text{ rad}$, which suggests the presence of broken-symmetry in nanomechanical resonators with $\theta < 0$. We attribute this to a change of built-in stress in the Si_3N_4 resonator from tension to compression, which, upon surpassing the buckling bifurcation point, breaks the out-of-plane symmetry and yields a buckled configuration (see SEM image in Fig. 3b). To verify these observations, we simulate the buckled resonator response by nonlinear reduced-order modeling of full FE models⁴⁰ and numerical continuation⁴¹ (see Supplementary Note 3), which had been successfully applied to model the nonlinear dynamics of graphene drums⁴⁰. It is worth mentioning that for a buckled string, the maximum amplitude does not always occur at the center of its first out-of-plane symmetric mode. Accordingly, we use FE simulations to obtain the amplitude ratio between the center of the mode and where it has the maximum amplitude, thus scaling the measured amplitudes at the center. The simulated results are shown as solid curves in Fig. 3a and demonstrate that the buckled

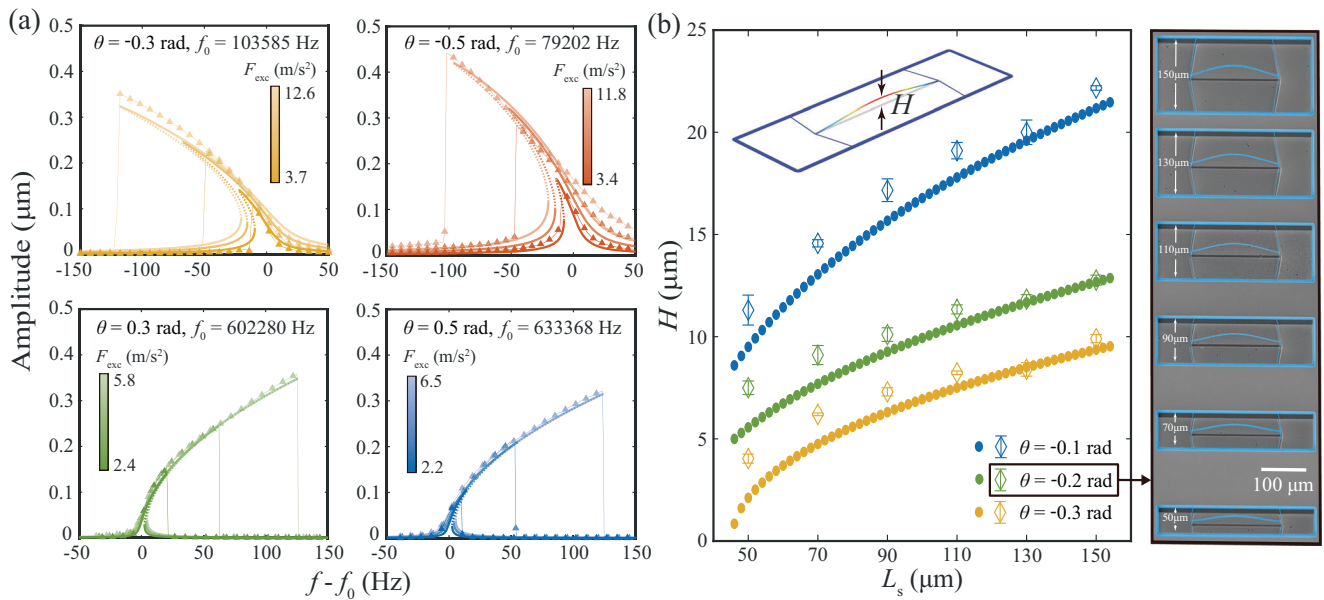


Fig. 3 | Influence of support angle θ on the geometric nonlinearity. **a** Finite element (FE) based (bold lines) and experimentally measured (triangles) frequency response curves of resonators with $w_s = 1 \mu\text{m}$ and $L_s = 150 \mu\text{m}$, showcasing the shifting between hardening and softening induced by the support angle θ . The solid parts of bold lines represent the stable branch of the simulated response, while the dotted parts are unstable. The legends show the mass-normalized drive level. The fitted β values for $\theta = (-0.3, -0.5)\text{rad}$ are $\beta = (-0.56, -0.27) \times 10^{22} \text{m}^{-2} \text{s}^{-2}$. For

$\theta = (0.3, 0.5)\text{rad}$, the Duffing constant $\beta = (7.00, 9.01) \times 10^{22} \text{m}^{-2} \text{s}^{-2}$. **b** Finite element (FE) based results (dots) and measurements (diamonds) of the buckling induced static displacement height H of the string at its center with $w_s = 1 \mu\text{m}$ for different support angles θ and lengths L_s . The inset shows the SEM image, colored in blue, of an array of buckled string resonators with $w_s = 1 \mu\text{m}$, $\theta = -0.2 \text{rad}$, and different L_s from $150 \mu\text{m}$ to $50 \mu\text{m}$.

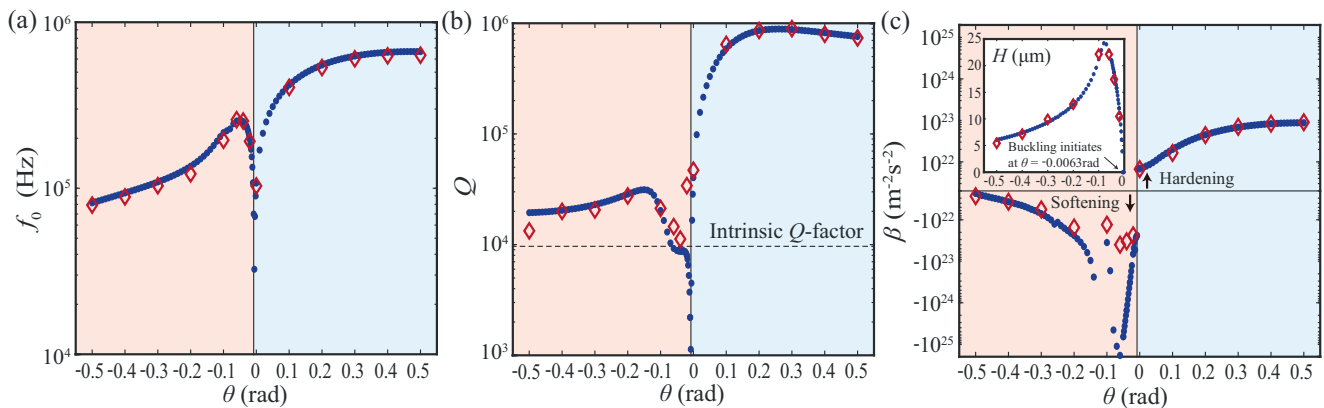


Fig. 4 | Tuning of the resonance frequency, Q -factor, and the effective geometric nonlinearity by varying support angles. Finite element (FE) based (dots) and measured (diamonds) **a** resonance frequencies f_0 , **b** Q -factors, and **c** geometric nonlinearity β of the first symmetric out-of-plane mode; note that the error bars are

smaller than the data marker size. The presented resonators share $L = 200 \mu\text{m}$, $w = 2 \mu\text{m}$, $w_s = 1 \mu\text{m}$, and $L_s = 150 \mu\text{m}$ but different support angles θ , which vary from -0.5rad to 0.5rad . The height of string center H is shown in (c) for negative θ .

configurations can account for the experimentally observed softening response (see Supplementary Note 3)⁴².

To further investigate the role of the support angle θ on the tunability of the dynamical properties, we perform additional measurements on string resonators with values of θ ranging from -0.5rad to 0.5rad while keeping $L_s = 150 \mu\text{m}$ and $w_s = 1 \mu\text{m}$ constant. In Fig. 4, we show the variation of the resonance frequency f_0 , Q -factor, and Duffing constant β of the first symmetric out-of-plane mode as a function of θ . We note that supports with positive θ significantly increase the values of the dynamical parameters shown in Fig. 4. This is attributed to higher k_{in} that results in higher tension and thus translates into higher values of f_0 , Q -factor, and the Duffing constant β (see Eq. (4)). The most intriguing observation, however, lies in the region where

the devices transition near $\theta = 0$ from a flat configuration to the buckled state. Here, we notice a sudden increase in the resonance frequency and the maximum $|\beta|$ of our devices, which is due to the large offset from the flat state (See Fig. 4a, c). By reducing θ towards -0.5rad , however, the post-buckling offset is found to decrease again, and subsequently, both f_0 and $|\beta|$ decrease monotonically. We noticed that near $\theta = 0$, the Q -factor of our devices drops to a similar level to that of stress-free string resonators⁴³, whose dissipation dilution disappears with the relaxation of high tension (see Fig. 4b)^{27,29}. However, we note that the FE-simulated Q -factor of devices close to the onset of buckling is lower than the intrinsic $Q_0 = 9864$. This could be attributed to the anti-spring behavior of the buckled strings that can result in $U_{total}/U_{bending} < 1$ and thus $Q < Q_0$ ^{29,44}. Included in Fig. 4c, we compare

experimental data to numerical results from reduced-order modeling of FE simulations that offer a higher θ resolution than experiments. The simulations (dots) are in good agreement with our experiments, except around $\theta = -0.1$ rad, where we faced numerical instability. We shall note that the simulations were conducted after a careful convergence study of the corresponding multi-mode reduced-order model, which also accounted for the broken symmetry induced by buckling. Furthermore, all the simulated results in Fig. 4 were obtained using the same material and geometric properties, and θ is the only parameter that is changed. The agreement between experiments and simulations is evident in the reliability of the modeling approach.

Discussion

The large tunability of the dynamical properties provided by geometric design offers new possibilities for engineering devices that are linear over a large range. For instance, as shown in Fig. 4, for devices with $\theta > 0$, it is possible to substantially decrease the geometric nonlinearity while maintaining a high Q -factor and thus expand the linear dynamic range of the resonator by increasing the onset of nonlinearity $a_{1\text{dB}} \propto Q^{-\frac{1}{2}}\alpha^{\frac{1}{2}}\beta^{-\frac{1}{2}}$ ^{45,46}. As an example, in devices with support angle θ around 0.1 rad, we note that both $a_{1\text{dB}}$ and Q -factor are three times higher than in conventional doubly clamped strings (see Supplementary Note 4). The methodology also provides the possibility to minimize β , such that it is infinitely small. We expect this condition to occur around $\theta = -0.0063$ rad according to FE simulations, where a transition from hardening to softening is observed. This condition is associated with the onset of buckling bifurcation when θ is varied, which is unstable and challenging to control, yet potentially possible to be stabilized by using external forces¹. On the other hand, it is desirable to operate devices in the nonlinear regime by squeezing the dynamic range (DR) of nanomechanical resonators (defined as the ratio $\text{DR} = 20\lg(a_{1\text{dB}}/a_{\text{th}})$, where a_{th} is the thermo-mechanical noise floor). Notably, in our current designs, we observe a reduction of DR from 64dB in a double-clamped string to 51dB in devices with slender supports. We foresee that by further reducing the thickness $h = 340$ nm of our devices, DR can even be squeezed down to near zero (see Supplementary Note 4), enabling the study of nonlinear dynamics in the Brownian limit⁴⁷. Moreover, recent studies have shown that by enhancing the ratio β/α , it is possible to realize nonlinear nanomechanical resonators that approach the quantum ground state in doubly clamped carbon nanotubes⁴⁸. Our simulations suggest that the absolute ratio of β/α in buckled resonators can be increased to an order of magnitude higher than that of double-clamped ones, suggesting that buckling can be used as an effective tool for increasing nonlinearities in modes that operate close to the quantum ground state⁴⁹.

In conclusion, we introduce a strategy to engineer the nonlinear dynamics of nanomechanical devices effectively by geometric design. We discuss the role of in-plane to out-of-plane coupling induced by the soft-clamping support, which we used to tune the geometric nonlinearity of high- Q string resonators down by two orders of magnitude compared to double-clamped strings. We also show that by carefully tuning the support angle, we can tune the stress in Si_3N_4 strings over the whole range from highly tensile to compressive, thus inducing a buckling bifurcation. We found that the post-buckled configurations show a softening nonlinearity with an absolute Duffing constant that increases with the buckling amplitude. The advantage of the presented nonlinear tuning method is that it does not require electrical or opto-thermal forces, providing a purely mechanical method for controlling nonlinear dynamics by design. This design is facilitated by the presented and validated analytic and finite element modeling techniques. Thus, the methodology allows for optimizing the dynamic range for each mechanical string resonator in the design phase, paving a robust way to realize large arrays of nanomechanical resonators with increased linearity or varying nonlinear functionalities for applications such as sensor arrays and quantum processing.

Methods

Sample fabrication

Devices are fabricated by electron beam lithography and reactive ion etching from high-stress Si_3N_4 layers. The layers are grown by

low-pressure chemical vapor deposition (LPCVD) with a thickness of $h = 340$ nm on a silicon substrate. The devices are then suspended by a fluorine-based (SF_6) deep reactive ion underetching step²⁷. All nanomechanical resonators studied in this work are made of Si_3N_4 deposited on the same wafer, which guarantees almost identical mechanical properties, with an initial isotropic stress $\sigma_0 = 1.06$ GPa, Young's modulus $E = 271$ GPa, Poisson's ratio $\nu = 0.23$, mass density $\rho = 3100$ kg/m³ and the intrinsic quality factor $Q_0 = 9864$. The resonance frequency f_0 and Q -factor characterization of these devices are detailed out in our previous work²⁹.

Data availability

The data that support the findings of this study are available from the corresponding authors upon reasonable request.

Code availability

Relevant codes are available from the corresponding authors upon reasonable request.

Received: 6 October 2023; Accepted: 25 January 2024;

Published online: 12 February 2024

References

1. Erbil, S. O. et al. Full electrostatic control of nanomechanical buckling. *Phys. Rev. Lett.* **124**, 046101 (2020).
2. Yuksel, M. et al. Nonlinear nanomechanical mass spectrometry at the single-nanoparticle level. *Nano Lett.* **19**, 3583–3589 (2019).
3. Okamoto, H., Mahboob, I., Onomitsu, K. & Yamaguchi, H. Rapid switching in high- Q mechanical resonators. *Appl. Phys. Lett.* **105**, 083114 (2014).
4. Bayram, F., Gajula, D., Khan, D. & Koley, G. Mechanical memory operations in piezotransistive GaN microcantilevers using an nanoparticle-enhanced photoacoustic excitation. *Microsyst. Nanoeng.* **8**, 1–14 (2022).
5. Okamoto, H., Mahboob, I., Onomitsu, K. & Yamaguchi, H. Rapid switching in high- q mechanical resonators. *Appl. Phys. Lett.* **105**, 083114 (2014).
6. Keşkekler, A. et al. Tuning nonlinear damping in graphene nanoresonators by parametric–direct internal resonance. *Nat. Commun.* **12**, 1–7 (2021).
7. Huber, J. S. et al. Spectral evidence of squeezing of a weakly damped driven nanomechanical mode. *Phys. Rev. X* **10**, 021066 (2020).
8. Villanueva, L. et al. Surpassing fundamental limits of oscillators using nonlinear resonators. *Phys. Rev. Lett.* **110**, 177208 (2013).
9. Chen, C., Zanette, D. H., Guest, J. R., Czaplowski, D. A. & López, D. Self-sustained micromechanical oscillator with linear feedback. *Phys. Rev. Lett.* **117**, 017203 (2016).
10. Miller, J. M., Gomez-Franco, A., Shin, D. D., Kwon, H.-K. & Kenny, T. W. Amplitude stabilization of micromechanical oscillators using engineered nonlinearity. *Phys. Rev. Res.* **3**, 033268 (2021).
11. Dou, S., Strachan, B. S., Shaw, S. W. & Jensen, J. S. Structural optimization for nonlinear dynamic response. *Philos. Trans. R. Soc. A* **373**, 20140408 (2015).
12. Antonio, D., Zanette, D. H. & López, D. Frequency stabilization in nonlinear micromechanical oscillators. *Nat. Commun.* **3**, 1–6 (2012).
13. Chen, C., Zanette, D. H., Czaplowski, D. A., Shaw, S. & López, D. Direct observation of coherent energy transfer in nonlinear micromechanical oscillators. *Nat. Commun.* **8**, 1–7 (2017).
14. Güttinger, J. et al. Energy-dependent path of dissipation in nanomechanical resonators. *Nat. Nanotechnol.* **12**, 631–636 (2017).
15. Davidovikj, D. et al. Nonlinear dynamic characterization of two-dimensional materials. *Nat. Commun.* **8**, 1253 (2017).
16. Steeneken, P. G., Dolleman, R. J., Davidovikj, D., Alijani, F. & Van der Zant, H. S. Dynamics of 2d material membranes. *2D Mater.* **8**, 042001 (2021).

17. Huang, L. et al. Frequency stabilization and noise-induced spectral narrowing in resonators with zero dispersion. *Nat. Commun.* **10**, 1–10 (2019).
18. Keskekler, A., Arjmandi-Tash, H., Steeneken, P. G. & Alijani, F. Symmetry-breaking-induced frequency combs in graphene resonators. *Nano Lett.* **22**, 6048–6054 (2022).
19. Czaplewski, D. A. et al. Bifurcation generated mechanical frequency comb. *Phys. Rev. Lett.* **121**, 244302 (2018).
20. Samanta, C., Arora, N. & Naik, A. Tuning of geometric nonlinearity in ultrathin nanoelectromechanical systems. *Appl. Phys. Lett.* **113**, 113101 (2018).
21. Sansa, M. et al. Frequency fluctuations in silicon nanoresonators. *Nat. Nanotechnol.* **11**, 552–558 (2016).
22. Villanueva, L. G. et al. A nanoscale parametric feedback oscillator. *Nano Lett.* **11**, 5054–5059 (2011).
23. Urgell, C. et al. Cooling and self-oscillation in a nanotube electromechanical resonator. *Nat. Phys.* **16**, 32–37 (2020).
24. Seis, Y. et al. Ground state cooling of an ultracoherent electromechanical system. *Nat. Commun.* **13**, 1507 (2022).
25. Sadeghi, P., Tanzer, M., Christensen, S. L. & Schmid, S. Influence of clamp-widening on the quality factor of nanomechanical silicon nitride resonators. *J. Appl. Phys.* **126**, 165108 (2019).
26. Fedorov, S. A., Beccari, A., Engelsen, N. J. & Kippenberg, T. J. Fractal-like mechanical resonators with a soft-clamped fundamental mode. *Phys. Rev. Lett.* **124**, 025502 (2020).
27. Shin, D. et al. Spiderweb nanomechanical resonators via bayesian optimization: inspired by nature and guided by machine learning. *Adv. Mater.* <https://doi.org/10.1002/adma.202106248> (2021).
28. Hoch, D., Yao, X. & Poot, M. Geometric tuning of stress in predisplaced silicon nitride resonators. *Nano Lett.* **22**, 4013–4019 (2022).
29. Li, Z. et al. Tuning the Q-factor of nanomechanical string resonators by torsion support design. *Appl. Phys. Lett.* **122**, 013501 (2023).
30. Li, L. L. et al. Tailoring the nonlinear response of mems resonators using shape optimization. *Appl. Phys. Lett.* **110**, 081902 (2017).
31. Cho, H. et al. Nonlinear hardening and softening resonances in micromechanical cantilever-nanotube systems originated from nanoscale geometric nonlinearities. *Int. J. Solids Struct.* **49**, 2059–2065 (2012).
32. Doster, J. et al. Observing polarization patterns in the collective motion of nanomechanical arrays. *Nat. Commun.* **13**, 2478 (2022).
33. Hatanaka, D., Mahboob, I., Onomitsu, K. & Yamaguchi, H. Phonon waveguides for electromechanical circuits. *Nat. Nanotechnol.* **9**, 520–524 (2014).
34. Bagheri, M., Poot, M., Fan, L., Marquardt, F. & Tang, H. X. Photonic cavity synchronization of nanomechanical oscillators. *Phys. Rev. Lett.* **111**, 213902 (2013).
35. Matheny, M. H. et al. Phase synchronization of two anharmonic nanomechanical oscillators. *Phys. Rev. Lett.* **112**, 014101 (2014).
36. Liu, J. et al. High-yield, wafer-scale fabrication of ultralow-loss, dispersion-engineered silicon nitride photonic circuits. *Nat. Commun.* **12**, 2236 (2021).
37. Nayfeh, A. H. & Mook, D. T. *Nonlinear Oscillations* (John Wiley & Sons, 2008).
38. Schmid, S., Villanueva, L. G. & Roukes, M. L. *Fundamentals of Nanomechanical Resonators*, vol. 49 (Springer, 2016).
39. Young, W. C., Budynas, R. G., Sadegh, A. M. et al. *Roark's Formulas for Stress and Strain*, vol. 7 (McGraw-Hill New York, 2002).
40. Keşkekler, A., Bos, V., Aragón, A. M., Steeneken, P. G. & Alijani, F. Multimode nonlinear dynamics of graphene resonators. *Phys. Rev. Applied.* **20**, 064020 (2023).
41. Dhooge, A., Govaerts, W., Kuznetsov, Y. A., Meijer, H. G. E. & Sautois, B. New features of the software matcont for bifurcation analysis of dynamical systems. *Math. Comput. Model. Dyn. Syst.* **14**, 147–175 (2008).
42. Lacarbonara, W., Nayfeh, A. H. & Kreider, W. Experimental validation of reduction methods for nonlinear vibrations of distributed-parameter systems: analysis of a buckled beam. *Nonlinear Dyn.* **17**, 95–117 (1998).
43. Villanueva, L. G. & Schmid, S. Evidence of surface loss as ubiquitous limiting damping mechanism in sin micro-and nanomechanical resonators. *Phys. Rev. Lett.* **113**, 227201 (2014).
44. Dykstra, D. M., Lenting, C., Masurier, A. & Coulais, C. Buckling metamaterials for extreme vibration damping. *Adv. Mater.* <https://doi.org/10.1002/adma.202301747> (2023).
45. Postma, H. C., Kozinsky, I., Husain, A. & Roukes, M. Dynamic range of nanotube-and nanowire-based electromechanical systems. *Appl. Phys. Lett.* **86**, 223105 (2005).
46. Molina, J. et al. High dynamic range nanowire resonators. *Nano Lett.* **21**, 6617–6624 (2021).
47. Barnard, A. W., Zhang, M., Wiederhecker, G. S., Lipson, M. & McEuen, P. L. Real-time vibrations of a carbon nanotube. *Nature* **566**, 89–93 (2019).
48. Samanta, C. et al. Nonlinear nanomechanical resonators approaching the quantum ground state. *Nat. Phys.* **19**, 1340–1344 (2023).
49. Geilhufe, R. M. Quantum buckling in metal-organic framework materials. *Nano Lett.* **21**, 10341–10345 (2021).

Acknowledgements

The research leading to these results received funding from the European Union's Horizon 2020 research and innovation program under Grant Agreement 802093 (ERC starting grant ENIGMA). Z.L. acknowledges financial support from the China Scholarship Council and the early assistance on the FE reduced-order modeling from Vincent Bos. This work is also part of the project, Probing the physics of exotic superconductors with microchip Casimir experiments (740.018.020) of the research program NWO Start-up, which is partly financed by the Dutch Research Council (NWO). M.X. and R.A.N. acknowledge valuable support from the Kavli Nanolab Delft.

Author contributions

Z.L., F.A., P.G.S., and A.M.A. conceived the experiments; M.X. and R.A.N. fabricated the Si₃N₄ samples; Z.L. conducted the measurements and analyzed the experimental data; Z.L. and F.A. built the theoretical model; Z.L. performed the reduced-order modeling of the finite element model; F.A. and P.G.S. supervised the project; and the paper was written by Z.L. and F.A. with inputs from all authors.

Competing interests

The authors declare no competing interests.

Additional information

Supplementary information The online version contains supplementary material available at <https://doi.org/10.1038/s42005-024-01543-7>.

Correspondence and requests for materials should be addressed to Zichao Li or Farbod Alijani.

Peer review information *Communications Physics* thanks the anonymous reviewers for their contribution to the peer review of this work. A peer review file is available.

Reprints and permissions information is available at <http://www.nature.com/reprints>

Publisher's note Springer Nature remains neutral with regard to jurisdictional claims in published maps and institutional affiliations.

Open Access This article is licensed under a Creative Commons Attribution 4.0 International License, which permits use, sharing, adaptation, distribution and reproduction in any medium or format, as long as you give appropriate credit to the original author(s) and the source, provide a link to the Creative Commons license, and indicate if changes were made. The images or other third party material in this article are included in the article's Creative Commons license, unless indicated otherwise in a credit line to the material. If material is not included in the article's Creative Commons license and your intended use is not permitted by statutory regulation or exceeds the permitted use, you will need to obtain permission directly from the copyright holder. To view a copy of this license, visit <http://creativecommons.org/licenses/by/4.0/>.

© The Author(s) 2024